Amorphous gallium oxide grown by low-temperature PECVD

Eiji Kobayashi, Mathieu Boccard, Quentin Jeangros, Nathan Rodkey, Daniel Vresilovic, Aïcha Hessler-Wyser, Max Döbeli, Daniel Franta, Stefaan De Wolf, Monica Morales-Masis, and Christophe Ballif

---

Articles you may be interested in

A review of Ga_2O_3 materials, processing, and devices
Applied Physics Reviews **5**, 011301 (2018); 10.1063/1.5006941

Guest Editorial: The dawn of gallium oxide microelectronics
Applied Physics Letters **112**, 060401 (2018); 10.1063/1.5017845

1-kV vertical Ga_2O_3 field-plated Schottky barrier diodes
Applied Physics Letters **110**, 103506 (2017); 10.1063/1.4977857

Enhancement-mode Ga_2O_3 wrap-gate fin field-effect transistors on native (100) β-Ga_2O_3 substrate with high breakdown voltage
Applied Physics Letters **109**, 213501 (2016); 10.1063/1.4967931

High breakdown electric field in β-Ga_2O_3/graphene vertical barristor heterostructure
Applied Physics Letters **112**, 032101 (2018); 10.1063/1.5002138

On the feasibility of p-type Ga_2O_3
Applied Physics Letters **112**, 032108 (2018); 10.1063/1.5009423

Amorphous gallium oxide grown by low-temperature PECVD

Eiji Kobayashi
École Polytechnique Fédérale de Lausanne (EPFL), Institute of Microengineering (IMT), Photovoltaics and Thin Film Electronics Laboratory, Rue de la Maladière 71b, CH-2002 Neuchâtel, Switzerland; Choshu Industry Co., Ltd., 3740, Shin-yamanoi, Sanyo Onoda, Yamaguchi 757-8511, Japan; and Department of Materials Science and Engineering, Yamaguchi University, 2-16-1 Tokiwadai, Ube, Yamaguchi 755-8611, Japan

Mathieu Boccard
École Polytechnique Fédérale de Lausanne (EPFL), Institute of Microengineering (IMT), Photovoltaics and Thin Film Electronics Laboratory, Rue de la Maladière 71b, CH-2002 Neuchâtel, Switzerland

Quentin Jeangros
École Polytechnique Fédérale de Lausanne (EPFL), Institute of Microengineering (IMT), Photovoltaics and Thin Film Electronics Laboratory, Rue de la Maladière 71b, CH-2002 Neuchâtel, Switzerland and Department of Physics, University of Basel, Klingelbergstrasse 82, CH-4056 Basel, Switzerland

Nathan Rodkey, Daniel Vresilovic, and Aïcha Hessler-Wyser
École Polytechnique Fédérale de Lausanne (EPFL), Institute of Microengineering (IMT), Photovoltaics and Thin Film Electronics Laboratory, Rue de la Maladière 71b, CH-2002 Neuchâtel, Switzerland

Max Döbeli
ETH Zurich, Ion Beam Physics, Otto-Stern-Weg 5, Zurich 8093, Switzerland

Daniel Franta
Department of Physical Electronics, Faculty of Science, Masaryk University, Kotlářská, 2, Brno 61137, Czechia

Stefaan De Wolf
KAUST Solar Center (KSC), King Abdullah University of Science and Technology (KAUST), Thuwal 23955-6900, Saudi Arabia

Monica Morales-Masis[a] and Christophe Ballif
École Polytechnique Fédérale de Lausanne (EPFL), Institute of Microengineering (IMT), Photovoltaics and Thin Film Electronics Laboratory, Rue de la Maladière 71b, CH-2002 Neuchâtel, Switzerland

Owing to the wide application of metal oxides in energy conversion devices, the fabrication of these oxides using conventional, damage-free, and upscalable techniques is of critical importance in the optoelectronics community. Here, the authors demonstrate the growth of hydrogenated amorphous gallium oxide (a-GaO$_x$:H) thin-films by plasma-enhanced chemical vapor deposition (PECVD) at temperatures below 200 °C. In this way, conformal films are deposited at high deposition rates, achieving high broadband transparency, wide band gap (3.5–4 eV), and low refractive index (1.6 at 500 nm). The authors link this low refractive index to the presence of nanoscale voids enclosing H$_2$, as indicated by electron energy-loss spectroscopy. This work opens the path for further metal-oxide developments by low-temperature, scalable and damage-free PECVD processes. *Published by the AVS.* https://doi.org/10.1116/1.5018800

I. INTRODUCTION

Gallium oxide (Ga$_2$O$_3$) is a wide band gap semiconductor with several crystalline phases; the most stable polymorph is the β structure, which has a band gap (E_g) of 4.5 to 4.9 eV,[1–3] the second largest E_g for semiconductors after diamond.[4] If nonstoichiometric, this phase is conductive with an electron mobility at 300 K up to 150 cm^2 V^{-1} s^{-1}.[5–8] β-Ga$_2$O$_3$ has potential applications as UV transparent electrodes[9] and field-effect transistors.[10,11] Recently, amorphous gallium oxide (a-GaO$_x$) with an E_g around 4 eV (Ref. 12) has drawn increased attention and was proposed as a transparent electron transport layer in Cu(In,Ga)Se$_2$ (Ref. 13) and

in Cu$_2$O (Ref. 14) solar cells as well as a passivation layer for c-Si solar cells.[15]

β-Ga$_2$O$_3$ can be deposited by several methods, including molecular beam epitaxy[16–18] and metal-organic chemical vapor deposition.[19–23] In all cases, high temperatures around 900–1050 °C are needed to obtain high-quality β-Ga$_2$O$_3$ thin films, limiting the choice of substrate. Gallium oxide can also be deposited at lower temperatures using plasma-enhanced atomic-layer deposition (PE-ALD),[24] yielding poorer crystalline quality or amorphous films. Notably, the growth of a-GaO$_x$ thin films was achieved by PE-ALD at temperatures in the range of 170–250 °C using trimethylgallium (TMG) and ozone (O$_3$) as reactants, with limited deposition rates though.[25,26]

Here, we demonstrate the use of plasma-enhanced chemical vapor deposition (PECVD) to grow a-GaO$_x$ using metal-organic precursors as an alternative, scalable approach to

these techniques. Compared to ALD, PECVD is a suitable method for mass production, with high deposition rates and scalability up to several square meters or even roll-to-roll. PECVD is industrially widespread, notably to manufacture amorphous silicon solar cells,[27] passivating layers in Si heterojunction (SHJ) solar cells,[28–34] and thin-film transistors of flat panel displays.[35] Importantly, PECVD tools developed for other types of layers are also suitable to fabricate GaO_x films. We demonstrate that transparent a-GaO_x films can be deposited by this method at a temperature of $200\,°C$. The optical properties, microstructure, surface morphology, and composition of the layers are studied, followed by testing this film as an antireflective coating (ARC) in SHJ solar cell.

II. EXPERIMENTAL SECTION

Substoichiometric hydrogenated a-GaO_x (a-GaO_x:H) films were deposited by PECVD using TMG as Ga precursor and carbon dioxide (CO_2) as oxidant in a custom-built PECVD reactor (originally designed for thin-film silicon deposition) operated at 70 MHz, 0.4 mbar, and $200\,°C$. A possible reaction between TMG and CO_2 is described as follows:

$$2\big[Ga(CH_3)_3\big]_{(g)} + 3[CO_2]_{(g)} \rightarrow [Ga_2O_3]_{(s)} + 3[CO]_{(g)}$$
$$+ 3[C_2H_6]_{(g)}. \qquad (1)$$
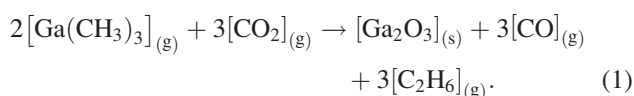
The oxidant (CO_2) gas flow to total gas flow ratio, Q_O, was set to be in the range of 93%–96%, with Q_O defined as

$$Q_O = \frac{CO_2\,gas\,flow}{CO_2\,gas\,flow + TMG\,gas\,flow}. \qquad (2)$$

The film thickness was varied between 2 and 800 nm depending on specific experimental or characterization method needs. The power-density of the plasma was 40 mW/cm^2, resulting in a deposition rate ranging from 0.7 to 1.1 nm/s for Q_O variations between 93% and 96%, respectively. For all investigated Q_O, all GaO_x films presented an amorphous microstructure as confirmed by X-ray diffraction (D2 PHASER, Bruker, data shown in supplementary material[61]).

The refractive indices (n) and extinction coefficients (k) of a-GaO_x:H films were determined with variable-angle spectroscopic ellipsometry measurements using a UVISEL ellipsometer (iHR320, HORIBA).[36] Photothermal deflection spectroscopy (PDS) with a custom-built system was used to determine the E_g and the absorption edge of the a-GaO_x:H films.[37,38] We used 800-nm-thick a-GaO_x:H films deposited on fused silica to maximize PDS signal and avoid glass absorption. Transmittance and absorptance spectra were measured with a spectrometer (Lambda 900, Perkin Elmer).

The conformality and microstructure of 50 nm-thick layers of a-GaO_x:H was assessed by transmission electron microscopy (TEM). Cross-sections of the layer stack were prepared using the conventional focused ion beam lift-out method (sample prepared in a Zeiss NVision) after these have been protected with evaporated carbon and sputtered Au to prevent FIB-induced damages. The TEM analysis involved the acquisition of STEM high-angle annular dark-field (HAADF) images that were combined with energy-dispersive X-ray spectroscopy (EDX) to assess the chemistry of the layers (in a FEI Tecnai Osiris microscope operated at 200 kV). In addition, GaO_x:H films with a thickness of 30 nm were deposited directly onto electron transparent 10-nm-thick SiN windows that were coated with 5 nm of C on their backside to prevent charging under the electron beam. Top view STEM dark-field (DF) images, electron energy-loss (EEL), and EDX spectra were acquired simultaneously to assess the composition of the film (using convergence and EELS collection semiangles of 28 and 48 mrad, respectively, in a FEI TITAN Themis at 80 kV). Additionally, the composition was assessed by Rutherford backscattering spectrometry (RBS) and by elastic recoil detection analysis (ERDA) as described in supplementary material.[39] The surface morphology was characterized by atomic force microscopy (AFM; Dimension Edge Scanasyst, Bruker).

Standard silicon heterojunction (SHJ) solar cells were fabricated using a-GaO_x:H as a second antireflecting (AR) layer to evaluate its effect in the optical performance of the solar cells (the conventional SHJ design uses a transparent conductive oxide, e.g., tin doped indium oxide (ITO), as the first AR layer).[40–43] Details on the SHJ cells fabrication can be found in Ref. 44. The a-GaO_x:H was deposited on such metalized devices using a shadow mask, covering the front-side ITO and metal fingers. A reference SHJ solar cell was fabricated with a thermally evaporated MgF_2 ARC. MgF_2 has been successfully applied as AR coating[45] in several record devices.[46,47] The current–voltage characteristics of these 4-cm^2 devices were measured under 1 kW/m^2 AM 1.5 G illumination and their spectral response with a custom-built setup.

III. RESULTS AND DISCUSSION

Figure 1(a) shows the transmittance and reflectance spectra of the a-GaO_x:H films deposited on fused silica, from which internal transmittance and absorptance are calculated and shown in Fig. 1(b), indicating that these films are transparent from the near UV to the near IR. This is confirmed by the low absorption coefficient (α) values measured by PDS. The α spectra of a-GaO_x:H films with Q_O from 93% to 96% are shown in Fig. 2(a). α is very low and decreases with increasing Q_O. E_g was extracted following the Tauc relation $\alpha = (hv - E_g)^x$, with hv the photon energy and $x = 1/2$, assuming direct optical transitions.[13,48] E_g varies from 3.5 to 4.1 eV when Q_O changes from 93% to 96% [Fig. 2(c)], indicating that E_g can be controlled by the oxidant gas flow during the deposition. Overall, the observed E_g of a-GaO_x:H is slightly lower than that of β-Ga_2O_3 (4.5–5.0 eV).[1–3]

Figure 3 shows n and k of a-GaO_x:H with Q_O from 93% to 96% obtained by ellipsometry using a universal dispersion model[49] (experimental spectra and fits are displayed in Fig. B.1 of the supplementary material). The static values of the dielectric function (relative permittivity, corresponding to only the electronic part of the dielectric response) of the a-GaO_x:H films with Q_O of 93%, 94%, 95%, and 96% were determined as 2.49, 2.42, 2.39, and 2.37, respectively. E_g
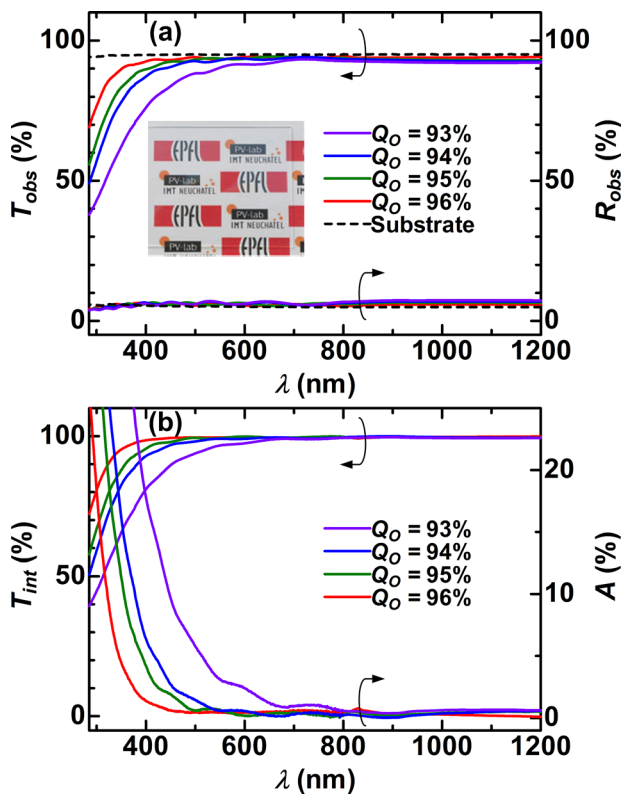
FIG. 1. (Color online) (a) Measured transmittance and reflectance spectra of a-GaO$_x$:H thin films with CO$_2$ gas to total flow ratios (Q_O) of 93%, 94%, 95%, and 96% (800 nm thickness on fused silica substrates). (b) Internal optical transmittance (T_{int}) and absorptance (A) calculated from T_{obs} and R_{obs} by $T_{int} = T_{obs}/(100 - R_{obs})$ and $A = 100 - T_{obs} - R_{obs}$. The inset in (a) shows a photograph of the a-GaO$_x$:H sample.

FIG. 2. (Color online) (a) PDS spectra, (b) Tauc plots, and (c) E_g values of a-GaO$_x$:H thin films with CO$_2$ gas to total flow ratios (Q_O) of 93%, 94%, 95%, and 96% (thickness of 800 nm, deposited on fused silica substrates).

values extracted from ellipsometry are slightly lower than those determined by PDS, which is attributed to the higher accuracy of the PDS in the UV part of the spectra with respect to the ellipsometry measurements.

The atomic content of Ga, O, C, and H in a-GaO$_x$:H films with Q_O of 95% (400-nm-thick on mirror-polished crystalline Si substrate) was analyzed by RBS and ERDA. An O/Ga ratio of 1.40 ± 0.10 was determined by RBS, indicating that the a-GaO$_x$:H films are slightly substoichiometric with respect to Ga$_2$O$_3$. ERDA measurements indicated a high H content of 31.7 ± 3.1 at. %, and a C/O ratio of 0.167 ± 0.012, corresponding to a C content of 6.0 ± 0.5 at. % homogeneously distributed in the bulk of the film (Fig. C.1. of supplementary material). The presence of H and C most likely originates from the use of TMG [Ga(CH$_3$)$_3$] and CO$_2$ gases.

The microstructure of thick (50 nm) and thin (2 nm) a-GaO$_x$:H with a Q_O of 95% was investigated by STEM imaging and EDX mapping. The a-GaOx:H layers were deposited on finished SHJ solar cells in two different configurations: thick (50 nm) a-GaO$_x$:H on top of ITO as ARC (Fig. 4) and thin (2 nm) a-GaOx:H between the a-Si:H and the ITO (see Fig. D1 of supplementary material[61]), to test whether it could be deposited as an electron transport layer, replacing the doped a-Si:H films in traditional SHJ solar cells in a dopant-free architecture.[50] Figure 4 displays the cross-
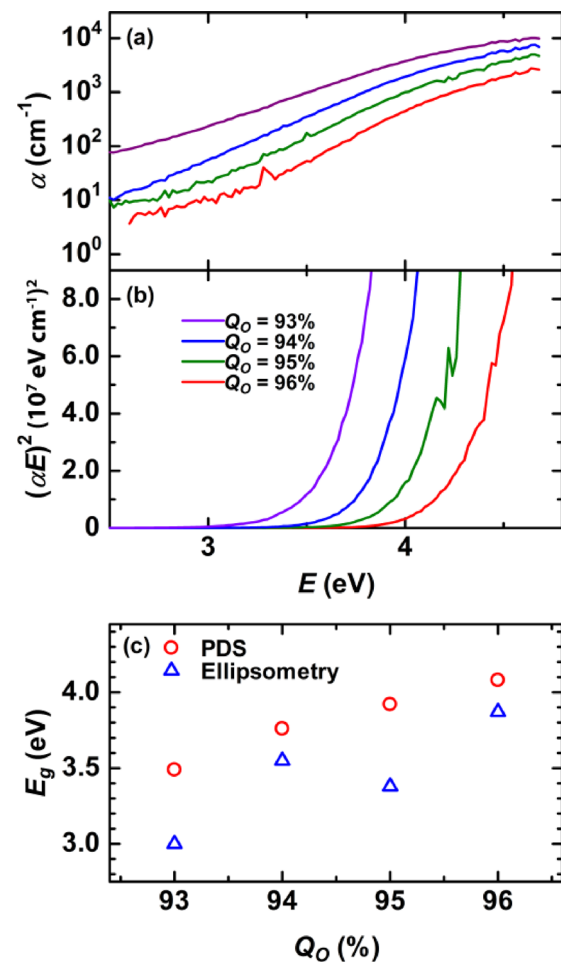
section TEM and EDX maps of the thick a-GaO$_x$:H deposited on a SHJ cell. Two regions of the pyramid shown in Fig. 4(a) are analyzed in more details; [(c) and (d)] showing one facet of the pyramid and (e) the valley of the pyramid. Both the electron micrograph and elemental distribution EDX maps indicate that the deposition of the a-GaO$_x$:H is mostly conformal. However, while still continuous, the film becomes thinner at the bottom of the valley between the pyramids, presumably due to shadowing effects, or lower adatom surface mobilities. The films are amorphous as shown by the high-resolution TEM micrograph and the Fourier transform shown in Fig. 4(d).

As suggested by the changes in contrast observed in Figs. 4(c) and 4(d), the top view DF image shown in Fig. 5(a) demonstrates the presence of small voids within the GaO$_x$:H film. Indeed, the regions of dark contrast contain voids as neither lighter elements in a solid form (see below) nor crystallites could be detected by EDX [Figs. 5(b) and 5(c)] or high-resolution TEM [as in Fig. 4(d)]. Interestingly, the regions with a darker DF contrast observed in Fig. 5(a) exhibit a small peak at 13.5 eV in the EEL spectrum. This small feature is highlighted in Fig. 5(d) by subtracting to the signal integrated in the range 12.5–15 eV a polynomial background
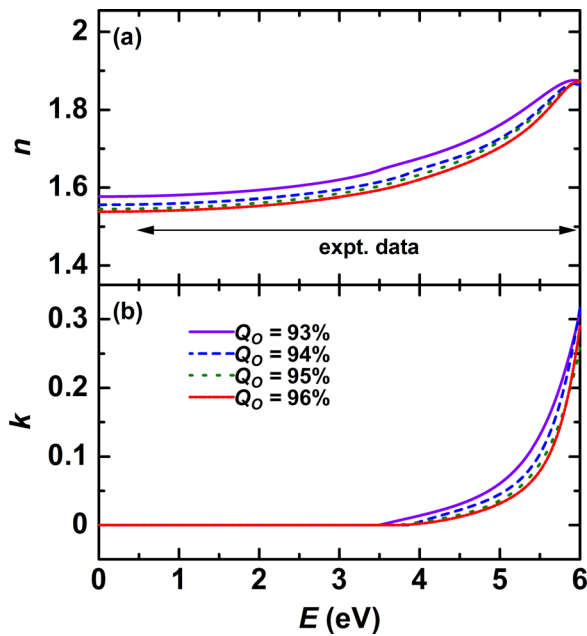
FIG. 3. (Color online) Optical constants of (a) refractive index n and (b) extinction coefficient k derived from the universal dispersion model fits of the ellipsometry measurements of a-GaO$_x$:H thin films grown with a CO_2 gas to total flow ratio (Q_O) of 93%, 94%, 95%, and 96%, respectively.

fitted in the energy ranges 11–12 and 15.5–17.5 eV. The procedure is illustrated in Fig. 5(e) for the EEL spectra taken at the positions of both a void/less dense region (red square on the left hand side) and a denser region (blue square on the right). Based on a comparison with literature data,[51] this small peak may correspond to the ionization K edge of the H_2 molecule

(13.6 eV). As demonstrated by the ERDA analysis detailed above, the film contains 31.7 ± 3.1 at. % of H. The EELS data hence tend to indicate that it is present in the film in the form H_2 trapped in (presumably) closed voids.

AFM was used to measure the surface morphology. Average surface roughness (R_a) and root-mean-square roughness (R_{ms}) of a-GaO$_x$:H films with Q_O of 93%–96% are shown in Table I and all below 1 nm, indicating that all films are very smooth.

As previously observed, the a-GaO$_x$:H films presented in this study show lower static n values (1.54–1.58) than β-Ga$_2$O$_3$ (1.89).[52] We speculate that the low n originates from the presence of nanosize voids as indicated by the TEM data (Figs. 4 and 5). Consistent with this, the results of RBS/ERDA also indicate a lower molecular density (1.3×10^{22} cm^{-3}) compared to the theoretical density of 1.9×10^{22} cm^{-3} in β-Ga$_2$O$_3$ calculated from the film density of 5.95 g cm^{-3}.[53] To further study the effect of H_2, we performed a series of depositions introducing additional H_2 during growth. Figure 6 shows n as a function of photon energy for the standard a-GaO$_x$:H films and films grown with 20 and 100 sccm additional H_2 flows. A slight refractive index increase (from 1.58 to 1.6 at 2.5 eV) is observed with increasing H_2 flow. As a tentative explanation, the introduction of additional H_2 in the plasma may etch the weak bonds at the growth surface of the film, resulting in denser films similarly to a-Si:H growth.[54] These three films were annealed at 200 °C with no change in optical properties, and then at 500 °C leading to an n increase of about 0.1 for all samples and a 20-nm thickness decrease. This is attributed to film reorganization, with the disruption of the nanosized voids resulting in a denser film
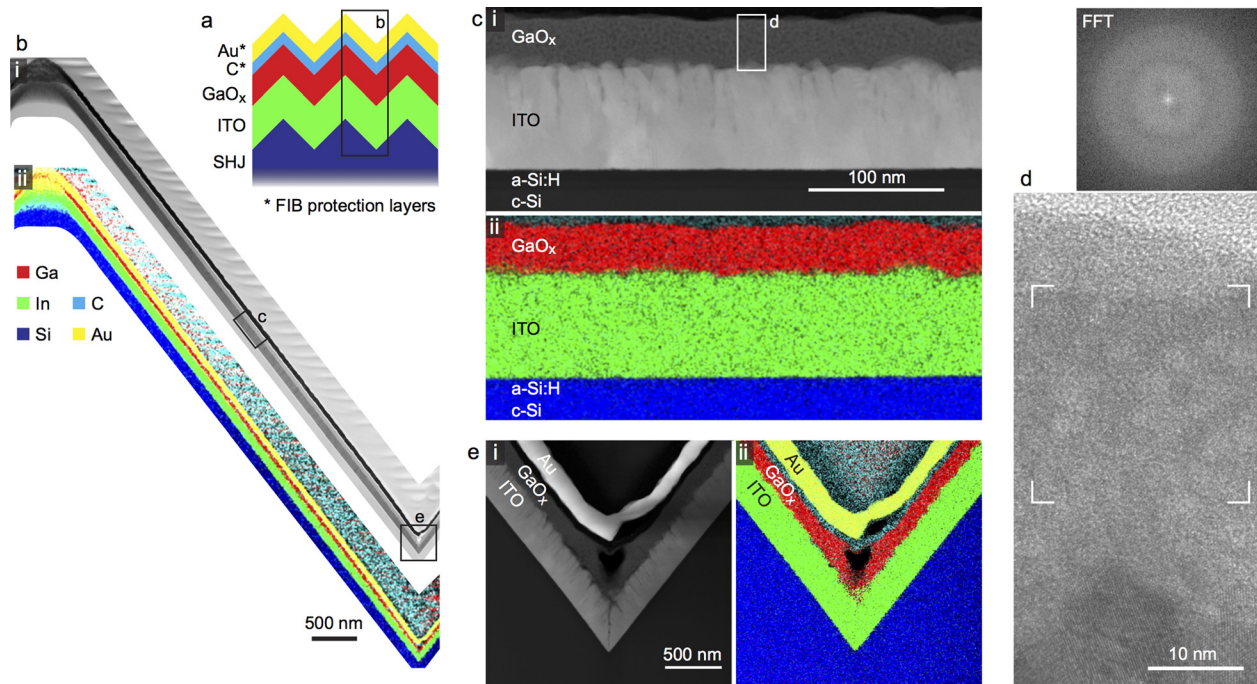

FIG. 4. (Color online) (a) Diagram of the layer stack. (b) STEM HAADF image and EDX map of one Si pyramid. (c)–(e) Higher magnification views of the GaO$_x$/ITO/a-Si:H stacks on [(c) and (d)] the flat side of the pyramid and (e) at the bottom of the pyramid, which show that a-GaO$_x$:H is conformal up until reaching the bottom of the valley, where it becomes thinner. The high-resolution TEM image of the a-GaO$_x$:H film and corresponding Fourier transform shown in (d) confirms the amorphous structure of the film.
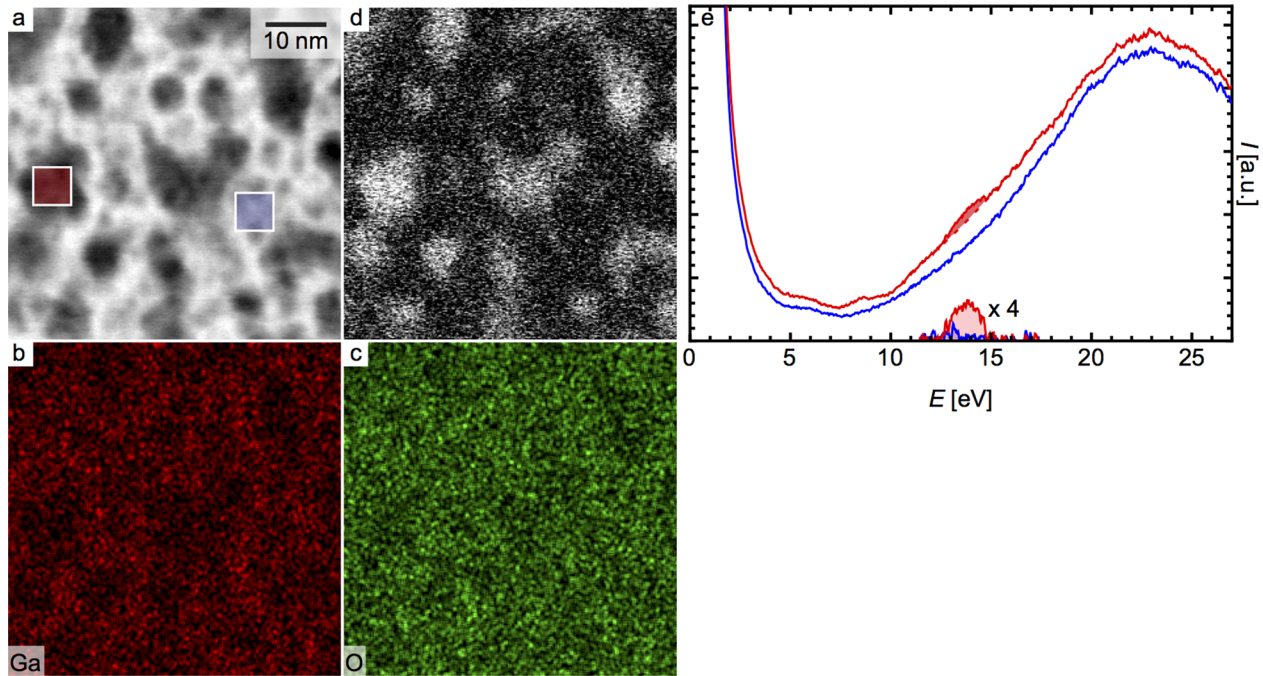
FIG. 5. (a) (Color online) STEM DF micrograph and corresponding EDX mapping of (b) Ga K and (c) O K edges. (d) EEL spectrum image obtained by subtracting a polynomial background to the EEL signal in the range 12–15.5 eV as colored in (e) for the EEL spectra taken either at the position of a void [red square on the left hand side in (a)] or a denser/brighter region (blue square on the right). The background-subtracted signals shown in (e) are magnified four times with respect to the full EEL spectra.

(still amorphous and porous though, based on TEM observations).

A straightforward application of the developed PECVD a-GaO$_x$:H—given the ideal combination of low refractive index (n of 1.57 at 500 nm) and broadband transparency—is its application as a dielectric layer for optoelectronic devices. For example, we investigated the potential of a-GaO$_x$:H as a second ARC layer on the front ITO of SHJ solar cells as shown in Fig. 7(b), similarly to the use of SiO$_x$.[55,56] SHJ solar cells with different ARC architectures were manufactured in CIC. The baseline SHJ cell without a second ARC had a short circuit current density (J_{sc}) of 39.1 mA cm^{-2}, an open circuit voltage of 722 mV, a fill factor of 82.2%, and a cell efficiency of 23.2%. The gain in J_{sc} due to the PECVD a-GaO$_x$:H coating [thickness (t) varied from 40 to 140 nm] on the front-side ITO layer ($t = 65$ nm) is shown in Fig. 7(a). A cell with a thermally evaporated MgF$_2$ ($t = 65$ nm, n of 1.37 at 500 nm)[57] second-layer ARC is also shown as reference. The 65-nm-thick a-GaO$_x$:H improves the J_{sc} by 0.47 mA cm^{-2} (0.27% efficiency gain in absolute), whereas the 65-nm-thick layer of MgF$_2$ increases the J_{sc} by 0.57 mA cm^{-2}, (0.33% efficiency gain in absolute). This difference originates from additional reflection in the 400 to 550 nm wavelength range (external quantum efficiency and reflectance spectra of the three cells shown in supplementary material, Fig. E1) and is due to the less-adequate refractive index of a-GaO$_x$:H compared to that of MgF$_2$ for solar cells measured in air.

TABLE I. Summary of the properties of a-GaO$_x$:H films deposited by PECVD with thicknesses (t) of 100 to 800 nm. The composition of the film grown with Q_O of 95% is Ga$_2$O$_{2.8}$C$_{0.46}$H$_{2.44}$.

|	Q_O			
Parameter	93%	94%	95%	96%
Phase ($t = 400$ nm on glass)	Amorphous	Amorphous	Amorphous	Amorphous
Static refractive index ($t = 100$ nm on c-Si)	1.58	1.56	1.55	1.54
Static dielectric constant ($t = 100$ nm on c-Si)	2.49	2.42	2.39	2.37
Bandgap E_g ($t = 800$ nm on fused silica)	3.49 eV	3.76 eV	3.92 eV	4.08 eV
O/Ga ratio ($t = 400$ nm on c-Si)	N/A	N/A	1.40 ± 0.10	N/A
C content ($t = 400$ nm on c-Si)	N/A	N/A	6.0 ± 0.5 at. %	N/A
H content ($t = 400$ nm on c-Si)	N/A	N/A	31.7 ± 3.1 at. %	N/A
Molecular density ($t = 400$ nm on c-Si)	N/A	N/A	1.38×10^{22} cm^{-3}	N/A
Average surface roughness R_a ($t = 200$ nm on glass)	0.350 nm	0.652 nm	0.588 nm	0.510 nm
Root-mean-square roughness R_{ms} ($t = 200$ nm on glass)	0.439 nm	0.794 nm	0.770 nm	0.648 nm
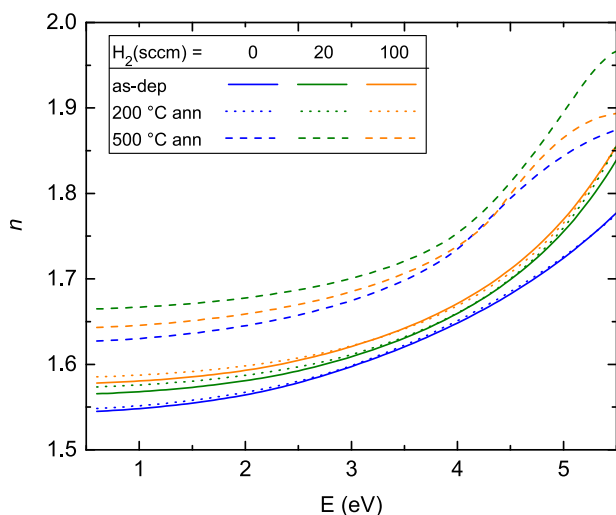
FIG. 6. (Color online) Refractive index (n) of a-GaO$_x$:H films grown with varying H_2 flows. n slightly increases with increasing H_2 flow, annealing in air at 200 °C causes no change in n, whereas annealing at 500 °C results in a clear increase of n for all samples.

IV. CONCLUSIONS

We introduced a PECVD process to deposit a-GaO$_x$:H thin films at low temperature (200 °C) and a detailed analysis of the film properties. The films are hydrogenated, amorphous, dielectric, highly transparent, slightly substoichiometric with respect to β-Ga$_2$O$_3$ and contain carbon, attributed to the use of TMG and CO_2 as gallium and oxidant precursors.
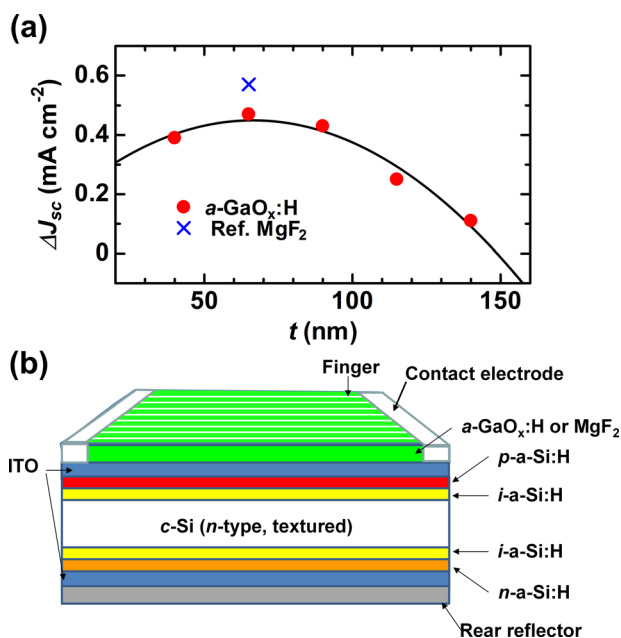

FIG. 7. (Color online) (a) Gain in J_{sc} of a SHJ cell as a function of the thickness of the a-GaO$_x$:H layer used as ARC on the front-side ITO ($t_{ITO} = 65$ nm). The gain in current when using a thermally evaporated MgF$_2$ ARC is marked by a cross. For each performance analysis, we measured the J-V characteristic of all cells before and after the a-GaO$_x$:H or MgF$_2$ ARC deposition. The solid line is the least-square quadratic fit for the a-GaO$_x$:H cells. (b) Schematic view of the Si heterojunction solar cell structure that employs a second ARC. All finger electrodes and contact electrodes are connected to the front side ITO layer.

A high oxidant content during PECVD was shown to increase the E_g up to 4.1 eV. Continuous films were obtained down to a thickness of 2 nm. The low refractive index below 1.6 could be linked to nanosized voids, which appear filled with molecular H_2. The potential of PECVD a-GaOx:H films as a second layer ARC in SHJ solar cells is demonstrated, and several other applications of PECVD a-GaO$_x$:H may be foreseen. For example, this material may also be used as an electron-transport material for photovoltaics, provided that extrinsic doping [e.g., Sn (Ref. 57) or Si (Ref. 58)] is added to improve the conductivity of the a-GaO$_x$:H. Alternatively, a-GaO$_x$:H with a low refractive index can replace MgF$_2$ as the rear reflector in SHJ cells.[59,60] Finally, the dielectric characteristics of the PECVD layers shown in this study are promising to apply as the dielectric in thin-film transistors. Furthermore, several aspects make PECVD an attractive method for the deposition of metal oxides, notably in the field of solar cells: softness of the deposition, extensive control of doping and stoichiometry, thickness control from nanometer to microns with the tunable deposition rate, and scalability and reliability at the industrial level, and this demonstration of PECVD-grown metal oxide could pave the road to the development of other PECVD metal oxide materials.

[1]H. H. Tippins, Phys. Rev. **140**, A316 (1965).

[2]M. Orita, H. Ohta, M. Hirano, and H. Hosono, Appl. Phys. Lett. **77**, 4166 (2000).

[3]T. Onuma, S. Fujioka, and T. Yamaguchi, Appl. Phys. Lett. **103**, 041910 (2013).

[4]M. Higashiwaki, K. Sasaki, A. Kuramata, T. Masui, and S. Yamakoshi, Appl. Phys. Lett. **100**, 013504 (2012).

[5]N. Ma, N. Tanen, A. Verma, Z. Guo, T. Luo, and H. Xing, Appl. Phys. Lett. **109**, 212101 (2016).

[6]K. Irmscher, Z. Galazka, M. Pietsch, R. Uecker, and R. Fornari, J. Appl. Phys. **110**, 063720 (2011).

[7]T. Oishi, Y. Koga, K. Harada, and M. Kazu, Appl. Phys. Express **8**, 031101 (2015).

[8]M. Higashiwaki, K. Sasaki, T. Kamimura, M. H. Wong, D. Krishnamurthy, A. Kuramata, T. Masui, and S. Yamakoshi, Appl. Phys. Lett. **103**, 123511 (2013).

[9]N. Ueda, H. Hosono, R. Waseda, and H. Kawazoe, Appl. Phys. Lett. **70**, 3561 (1997).

[10]F. Ren, M. Hong, S. N. G. Chu, M. A. Marcus, M. J. Schurman, A. Baca, S. J. Pearton, and C. R. Abernathy, Appl. Phys. Lett. **73**, 3893 (1998).

[11]K. D. Chabak *et al.*, Appl. Phys. Lett. **109**, 213501 (2016).

[12]M. D. Heinemann, J. Berry, G. Teeter, T. Unold, and D. Ginley, Appl. Phys. Lett. **108**, 022107 (2016).

[13]T. Koida, Y. Kamikawa-Shimizu, A. Yamada, H. Shibata, and S. Niki, IEEE J. Photovoltaics **5**, 956 (2015).

[14]T. Minami, Y. Nishi, and T. Miyata, Appl. Phys. Express **6**, 044101 (2013).

[15]T. G. Allen, Y. Wan, and A. Cuevas, IEEE J. Photovoltaics **6**, 900 (2016).

[16]E. G. Víllora, K. Shimamura, K. Kitamura, and K. Aoki, Appl. Phys. Lett. **88**, 031105 (2006).

[17]K. Sasaki, A. Kuramata, T. Masui, E. G. Villora, K. Shimamura, and S. Yamakoshi, Appl. Phys. Express **5**, 035502 (2012).

[18]P. Vogt and O. Bierwagen, Appl. Phys. Lett. **106**, 081910 (2015).

[19]M. Valet and D. M. Hoffman, Chem. Mater. **13**, 2135 (2001).

[20]R. Binions, C. J. Carmalt, I. P. Parkin, and K. F. E. Pratt, Chem. Mater. **16**, 2489 (2004).

[21]H. W. Kim and N. H. Kim, Appl. Phys. A **81**, 763 (2005).

[22]C. Y. Huang, R. H. Horng, D. S. Wuu, L. W. Tu, and H. S. Kao, Appl. Phys. Lett. **102**, 011119 (2013).

[23]D. Gogova, G. Wagner, M. Baldin, M. Schmidbauer, K. Irmscher, R. Schewski, Z. Galazka, M. Albrecht, and R. Fornari, J. Cryst. Growth **401**, 665 (2014).

[24]C. L. Dezelah, J. Niinisto, K. Arstila, L. Niinisto, and C. H. Winter, Chem. Mater. **18**, 471 (2006).

[25]D. J. Comstock and J. W. Elam, Chem. Mater. **24**, 4011 (2012).

[26]T. G. Allen and A. Cuevas, Appl. Phys. Lett. **105**, 031601 (2014).

[27]A. Shah, P. Torres, R. Tscharner, N. Wyrsch, and H. Keppner, Science **285**, 692 (1999).

[28]K. Yoshikawa *et al.*, Nat. Energy **2**, 17032 (2017).

[29]D. Adachi, J. L. Hernandez, and K. Yamamoto, Appl. Phys. Lett. **107**, 233506 (2015).

[30]K. Masuko *et al.*, IEEE J. Photovoltaics **4**, 1433 (2014).

[31]M. Taguchi, A. Yano, S. Tohoda, K. Matsuyama, Y. Nakamura, T. Nishiwaki, K. Fujita, and E. Maruyama, IEEE J. Photovoltaics **4**, 96 (2013).

[32]H. Fujiwara and M. Kondo, Appl. Phys. Lett. **90**, 013503 (2007).

[33]S. De Wolf and M. Kondo, Appl. Phys. Lett. **90**, 042111 (2007).

[34]S. De Wolf, C. Ballif, and M. Kondo, Phys. Rev. B **85**, 113302 (2012).

[35]R. A. Street, Adv. Mater. **21**, 2007 (2009).

[36]H. Tompkins and E. A. Irene, *Handbook of Ellipsometry* (William Andrew, New York, 2005), pp. 3–90.

[37]S. De Wolf, J. Holovsky, S. J. Moon, P. Loper, B. Niesen, M. Ledinsky, F. J. Haug, J. H. Yum, and C. Ballif, J. Phys. Chem. Lett. **5**, 1035 (2014).

[38]M. Morales-Masis, S. M. De Nicolas, J. Holovsky, S. De Wolf, and C. Ballif, IEEE J. Photovoltaics **5**, 1340 (2015).

[39]C. Kottler, M. Dobeli, F. Glaus, and M. Suter, Nucl. Instrum. Methods, B **248**, 155 (2006).

[40]S. De Wolf, A. Descoeudres, Z. C. Holman, and C. Ballif, Green **2**, 7 (2012).

[41]S. Y. Lien, Thin Solid Films **518**, S10 (2010).

[42]M. Balestrieri, D. Pysch, J. P. Becker, M. Hermle, W. Warta, and S. W. Glunz, Sol. Energy Mater. Sol. Cells **95**, 2390 (2011).

[43]M. Morales-Masis, S. De Wolf, R. Woods-Robinson, J. W. Ager, and C. Ballif, Adv. Electron. Mater. **3**, 1600529 (2017).

[44]E. Kobayashi, S. De Wolf, J. Levrat, G. Christmann, A. Descoeudres, S. Nicolay, and M. Despeisse, Appl. Phys. Lett. **109**, 153503 (2016).

[45]P. Campbell, S. R. Wenham, and M. A. Green, Sol. Energy Mater. Sol. Cells **31**, 133 (1993).

[46]J. Zhao, A. Wang, P. P. Altermatt, S. R. Wenham, and M. A. Green, Sol. Energy Mater. Sol. Cells **41/42**, 87 (1996).

[47]P. Jackson, D. Hariskos, E. Lotter, S. Paetel, R. Wuerz, R. Menner, W. Wischmann, and M. Powalla, Prog. Photovoltaics **19**, 894 (2011).

[48]J. I. Pankove, *Optical Processes in Semiconductors* (Dover Publications, Inc., New York, 1971).

[49]D. Franta, D. Nečas, and I. Ohlídal, Appl. Opt. **54**, 9108 (2015).

[50]J. Bullock *et al.*, Nat. Energy **1**, 15031 (2016).

[51]C. C. Ahn and O. L. Krivanek, *EELS Atlas: A Reference Collection of Electron Energy Loss Spectra Covering All Stable Elements* (Gatan, Inc., Warrendale, PA, 1983).

[52]M. Rebien, W. Henrion, M. Hong, and J. P. Mannaerts, Appl. Phys. Lett. **81**, 250 (2002).

[53]A. Gyekenyesi and M. Halbig, *Ceramic Materials for Energy Applications IV: Ceramic Engineering and Science Proceedings* (Wiley, Hoboken, NJ, 2014). Vol. 35, No. 7.

[54]J. H. Koh, Y. H. Lee, H. Fujiwara, and C. R. Wronski, Appl. Phys. Lett. **73**, 1526 (1998).

[55]D. Zhang, I. A. Digdaya, R. Santbergen, R. A. C. M. M. van Swaaij, P. Bronsveld, M. Zeman, J. A. M. van Roosmalen, and A. W. Weeber, Sol. Energy Mater. Sol. Cells **117**, 132 (2013).

[56]S. Y. Herasimenka, W. J. Dauksher, M. Boccard, and S. Bowden, Sol. Energy Mater. Sol. Cells **158**, 98 (2016).

[57]N. Suzuki, S. Ohira, M. Tanaka, T. Sugawara, K. Nakajima, and T. Shishido, Phys. Status Solidi (c) **4**, 2310 (2007).

[58]S. Müller, H. von Wenckstern, D. Splith, F. Schmidt, and M. Grundmann, Phys. Status Solidi (a) **211**, 34 (2014).

[59]Z. C. Holman, A. Descoeudres, S. De Wolf, and C. Ballif, IEEE J. Photovoltaics **3**, 1243 (2013).

[60]A. Dabirian, M. Morales-Masis, F. J. Haug, S. De Wolf, and C. Ballif, IEEE J. Photovoltaics **7**, 718 (2017).

[61]See supplementary material at https://doi.org/10.1116/1.5018800 for details of XRD, ERDA, ellipsometry fitting data and STEM analysis.